Quantum Entanglement of High Angular Momenta

Robert Fickler *et al.*

Science **338**, 640 (2012);
DOI: 10.1126/science.1227193

test photon created by the detection of the corroborative photon, the presence of entanglement must be verified (*16*, *21*). Note that several recent works did not do this; therefore, the presence of a QBS has not been proven unambiguously (*22*, *23*). In our realization, entanglement is proven by performing the same experiment as before, but using the complementary analysis basis, namely the diagonal basis $\{D, A\}$. Now, the initial quantum state is rotated by 45°—i.e., $\frac{1}{\sqrt{2}}(c_V^\dagger t_V^\dagger + c_H^\dagger t_H^\dagger)|vac\rangle \rightarrow \frac{1}{\sqrt{2}}(c_D^\dagger t_D^\dagger + c_A^\dagger t_A^\dagger)|vac\rangle$—where D and A symbolize diagonally and antidiagonally polarized photon contributions, respectively. In this configuration, every single photon is unpredictably subjected to a closed or open Mach-Zehnder configuration by the PDBS. In this case, as opposed to the experiment in the $\{H, V\}$ basis, if a statistical mixture was analyzed instead of an entangled state, no correlations should be observed when measuring $I_{H,b}(\theta,\alpha)$. However, the strong correlations shown in Fig. 4C exclude a statistical mixture and are in good agreement with the theoretical predictions of Eq. 6. This emphasizes that wave and particle behavior coexist simultaneously for the entire range $0° < \alpha < 90°$ in the $\{H, V\}$ basis and for $-45° < \alpha < 45°$ in the $\{D, A\}$ basis. Figure 4D shows the measurements for V^2, D^2, and $V^2 + D^2$ as a function of α and confirms the upper limits imposed by Eq. 7. The quality of the entangled state is measured via the Bell parameter S, which is deduced from the phase oscillation visibilities at $\alpha = 90°$ in the $\{H, V\}$ basis and $\alpha = 45°$ in the $\{D, A\}$ basis. We obtain $S = 2.77 \pm 0.07$, which is very close to the optimal value of $2\sqrt{2}$ attained with maximally entangled states and is 11 standard deviations above the classical/quantum boundary $S = 2$ (*16*, *21*).

The detection loophole remains open in our experiment, because some of the initial entangled photons are lost during their propagation in the fiber or bulk channels or are not detected by the single-photon detectors that show nonunit quantum detection efficiencies (*24*). Therefore, we make the reasonable assumption that the detected photons represent a faithful sample (*17*).

In conclusion, we have carried out a quantum delayed-choice experiment, enabled by polarization-entangled photons and the associated property of nonlocality. We used an MZI in which the output beam splitter has been replaced by its quantum analog (i.e., a beam splitter in a coherent superposition of being present and absent). In this configuration, we observed that single photons can behave as waves and as particles in the same experiment, meaning that the simple view of photons being either waves or particles is refuted. We experimentally excluded interpretations based on local hidden variables and/or information exchange between the photon and the quantum beam splitter. The state of the quantum beam splitter is determined by the detection of the corroborative photon. We have, therefore, demonstrated delayed interference between wave and particle behavior, which underlines the subtleness of Bohr's complementarity principle.

We note that, parallel to this work, Peruzzo *et al.* realized another version of a quantum delayed-choice experiment based on entangled photons (*25*).

References and Notes

1. E. Schrödinger, *Naturwissenschaften* **23**, 807 (1935).
2. G. Greenstein, A. Zajonc, *The Quantum Challenge: Modern Research on the Foundations of Quantum Mechanics* (Jones and Bertlett Publishers, Sudbury, MA, 2006).
3. N. Bohr, in *Quantum Theory and Measurement*, J. A. Wheeler, W. H. Zurek, Eds. (Princeton Univ. Press, Princeton, NJ, 1984), p. 949.
4. Y.-H. Kim, R. Yu, S. P. Kulik, Y. Shih, M. O. Scully, *Phys. Rev. Lett.* **84**, 1 (2000).
5. S. P. Walborn, M. O. Terra Cunha, S. Pádua, C. H. Monken, *Phys. Rev. A* **65**, 033818 (2002).
6. P. Grangier, G. Roger, A. Aspect, *Europhys. Lett.* **1**, 173 (1986).
7. J. A. Wheeler, in *Quantum Theory and Measurement*, J. A. Wheeler, W. H. Zurek, Eds. (Princeton Univ. Press, Princeton, NJ, 1984), pp. 182–213.
8. V. Jacques *et al.*, *Science* **315**, 966 (2007).
9. W. K. Wootters, W. H. Zurek, *Phys. Rev. D* **19**, 473 (1979).
10. B.-G. Englert, *Phys. Rev. Lett.* **77**, 2154 (1996).
11. V. Jacques *et al.*, *Phys. Rev. Lett.* **100**, 220402 (2008).
12. J.-S. Tang *et al.*, *Nat. Photonics* **6**, 602 (2012).
13. R. Ionicioiu, D. R. Terno, *Phys. Rev. Lett.* **107**, 230406 (2011).
14. M. Schirber, *Physics* **4**, 102 (2011).
15. A. Einstein, B. Podolsky, N. Rosen, *Phys. Rev.* **47**, 777 (1935).
16. J. S. Bell, *Physics* **1**, 195 (1964).
17. A. Aspect, J. Dalibard, G. Roger, *Phys. Rev. Lett.* **49**, 1804 (1982).
18. G. Weihs, T. Jennewein, C. Simon, H. Weinfurter, A. Zeilinger, *Phys. Rev. Lett.* **81**, 5039 (1998).
19. F. Kaiser, A. Issautier, O. Alibart, A. Martin, S. Tanzilli, *Phys. Rev. Lett.* **75**, 3034 (1995).
21. J. F. Clauser, M. A. Horne, A. Shimony, R. A. Holt, *Phys. Rev. Lett.* **23**, 880 (1969).
22. S. S. Roy, A. Shukla, T. S. Mahesh, *Phys. Rev. A* **85**, 022109 (2012).
23. R. Auccaise *et al.*, *Phys. Rev. A* **85**, 032121 (2012).
24. J. F. Clauser, M. A. Horne, *Phys. Rev. D Part. Fields* **10**, 526 (1974).
25. A. Peruzzo, P. Shadbolt, N. Brunner, S. Popescu, J. L. O'Brien, *Science* **338**, 634 (2012).
26. X.-S. Ma *et al.*, *Nat. Phys.* **8**, 480 (2012).

Acknowledgments: We thank L. A. Ngah for his help on data acquisition and O. Alibart for fruitful discussions. This work was supported by the CNRS, l'Université de Nice–Sophia Antipolis, l'Agence Nationale de la Recherche for the "e-QUANET" project (grant ANR-09-BLAN-0333-01), the European ICT-2009.8.0 FET open program for the "QUANTIP" project (grant 244026), le Ministère de l'Enseignement Supérieur et de la Recherche, la Fondation iXCore pour la Recherche, and le Conseil Régional PACA for the "QUANET" project in the exploratory call.

Supplementary Materials

www.sciencemag.org/cgi/content/full/338/6107/637/DC1
Supplementary Text
Fig. S1

29 June 2012; accepted 18 September 2012
10.1126/science.1226755

Quantum Entanglement of High Angular Momenta

Robert Fickler,[1,2]* Radek Lapkiewicz,[1,2] William N. Plick,[1,2] Mario Krenn,[1,2] Christoph Schaeff,[1,2] Sven Ramelow,[1,2] Anton Zeilinger[1,2,3]*

Single photons with helical phase structures may carry a quantized amount of orbital angular momentum (OAM), and their entanglement is important for quantum information science and fundamental tests of quantum theory. Because there is no theoretical upper limit on how many quanta of OAM a single photon can carry, it is possible to create entanglement between two particles with an arbitrarily high difference in quantum number. By transferring polarization entanglement to OAM with an interferometric scheme, we generate and verify entanglement between two photons differing by 600 in quantum number. The only restrictive factors toward higher numbers are current technical limitations. We also experimentally demonstrate that the entanglement of very high OAM can improve the sensitivity of angular resolution in remote sensing.

Quantum entanglement—the nonclassical phenomenon of joint measurements of at least two separate systems showing stronger correlations than classically explainable (*1*, *2*)—is widely considered one of the quintessential features of quantum theory. Since its discovery and first experimental demonstration (*3*), photon entanglement has been shown in various degrees of freedom (*4*–*7*). In the field of photonic quantum optics, studies of the orbital angular momentum (OAM) of light have been productive. The natural solutions of the paraxial wave equation in cylindrical coordinates, Laguerre-Gauss modes, have a helical phase dependence that leads to a vortex or phase singularity and thus zero intensity along the beam axis. These Laguerre-Gauss modes carry an OAM that can take any integer value (*8*). Entanglement of OAM of photons (*5*) has led to many novel insights and applications in quantum foundations and quantum information—for example, qutrit quantum com-

[1]Quantum Optics, Quantum Nanophysics, Quantum Information, University of Vienna, Vienna A-1090, Austria. [2]Institute for Quantum Optics and Quantum Information, Austrian Academy of Science, Vienna A-1090, Austria. [3]Vienna Center for Quantum Science and Technology, Faculty of Physics, University of Vienna, Vienna A-1090, Austria.

*To whom correspondence should be addressed. E-mail: robert.fickler@univie.ac.at (R.F.); anton.zeilinger@univie.ac.at (A.Z.)

munication protocols (*9*), uncertainty relations with angular position and OAM (*10*), or higher-dimensional entanglement (*11*–*13*).

An important motivation for our work is the open question of the existence of macroscopic entanglement, which is intricately connected to the very definition of "macroscopicity" (*14*). The OAM degree of freedom offers the possibility to create entanglement of quantum numbers in principle up to arbitrarily high values. In optomechanical experiments, which already make use of linear momentum (*15*), such photons can be used to create entanglement of a mechanical system with high angular momentum. Also, relative to classical methods, quantum remote sensing offers an improved angular resolution that is amplified by large OAM values (*16*).

Because of the rapidly decreasing efficiency of the downconversion process for the direct generation of entanglement of higher OAM (*17*, *18*), we use a different approach similar to the ideas in (*7*, *19*–*21*). We start with high-fidelity two-dimensional entanglement in the polarization degrees of freedom and transfer it to various OAM subspaces with chosen amounts of angular momentum (Fig. 1). The polarization-entangled photon pairs propagating in single-mode fibers enter the transfer setups in the two-photon state described by the tensor product of two degrees of freedom (polarization and OAM):

$$|\psi_{in}\rangle = [\alpha|H\rangle|V\rangle + \beta \exp(i\varphi)|V\rangle|H\rangle]\otimes|0\rangle|0\rangle \quad (1)$$

where α, β, and φ are real and normalized ($\alpha^2 + \beta^2 = 1$), H and V denote horizontal and vertical polarization, 0 indicates the amount of OAM per photon (Gauss mode), and the positions of the ket vectors, which describe the quantum mechanical states of the photon, label the different photons. The transfer is realized with a folded interferometric structure that is intrinsically phase-stable and has by design equal arm lengths. Depending on their polarization, the photons are transferred to a well-defined Laguerre-Gauss mode by a spatial light modulator (SLM), which modulates the phase of the light (*22*). The SLM is programmed such that photons that take the path for horizontally polarized light are changed to $+l$ after leaving the interferometer, and those that take the path for vertically polarized light are changed to $-l$ after leaving the interferometer. Finally, a polarizer projects the photons onto the diagonal polarization (D), erasing any information about path and creating the state

$$|\psi_{out}\rangle = |D\rangle|D\rangle\otimes[|\alpha| + l\rangle|-l\rangle + \beta \exp(i\varphi)|-l\rangle|+l\rangle] \quad (2)$$

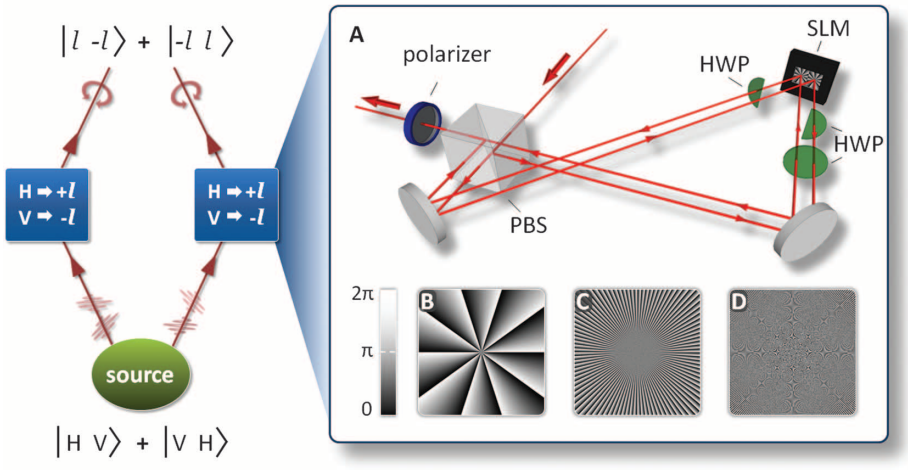

Fig. 1. Left panel: Schematic sketch of the setup. Polarization entanglement is created in a parametric downconversion process (source) and afterward transferred to modes with high quanta of OAM (transfer setups, shown as blue boxes). (**A**) Experimental layout for one of the two identical transfer setups where the photon is split by a polarization beam splitter (PBS) and its spatial mode is transformed to a higher-order Laguerre-Gauss mode by a spatial light modulator (SLM). Half-wave plates (HWP) in the paths ensure that the SLM works optimally and that the output is separated from the input. A polarizer (blue) projects the photon to diagonal polarization and completes the transfer. (**B** to **D**) Three-phase pattern of increasing complexity of the structure: l = 10 (B), l = 100 (C), and l = 300 (D). Because the SLM has finite resolution, a Moiré pattern emerges.

Our method does not rely on phase matching, as in the generation of OAM entanglement via spontaneous parametric downconversion (SPDC), but instead benefits from the efficient and high-quality polarization entanglement. The resulting states can be entangled in any two-dimensional subspace of the infinite-dimensional OAM space or even in the general space of all spatial modes that can be generated with SLMs (*23*–*25*).

To realize projective measurements onto high-OAM superposition states in order to demonstrate entanglement, we use a technique that takes advantage of the specific spatial structure of the created photonic states (Fig. 2). Any equal Laguerre-Gauss superposition, $|\chi\rangle = 2^{-1/2}[|l\rangle + \exp(i\varphi)|-l\rangle]$, has an intensity distribution showing a radially symmetric structure with $2l$ maxima arranged in a ring (Fig. 2, B to D). Because the angular position $\gamma = (\varphi/2l)\cdot(360°/2\pi)$ of this petal structure is determined by the phase φ, a mask with $2l$ slits maximally transmits only a specific superposition. By rotating the mask, all possible superpositions with equal amplitude are accessible. For analysis of the created state and demonstration of entanglement, one mask is installed after each transfer setup

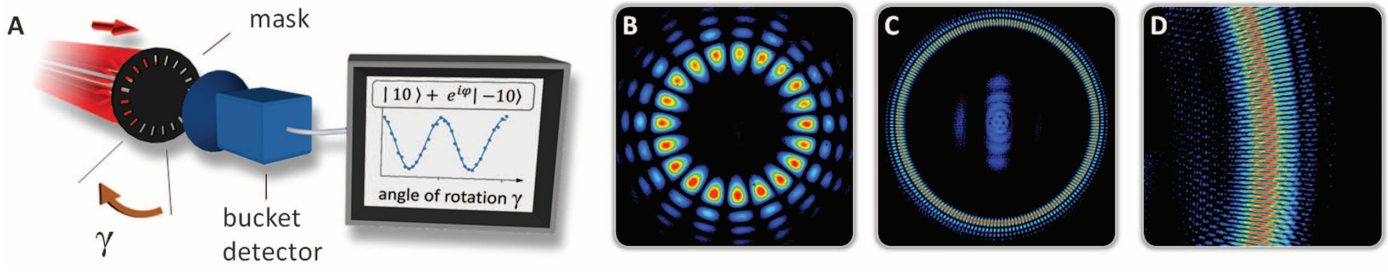

Fig. 2. Sketch of the measurement principle. (**A**) The angular position of the radial superposition structure (red) is dependent on the phase φ of the state, here $|\chi\rangle = |10\rangle + \exp(i\varphi)|-10\rangle$. A mask with the same rotational symmetry (20 slits) is able to detect any superposition depending on the mask's angular position γ. (**B** to **D**) Three superpositions (false colors denote intensity gradations) for $l = \pm 10$ (B), $l = \pm 100$ (C), and a section of the mode for $l = \pm 300$ (D), experimentally created with a laser imaged by a charge-coupled device camera. Additional structures around and inside of the main intensity pattern (higher-order Laguerre-Gauss modes with the same OAM and unmodulated photons, respectively) arise from the imperfect creation of the modes at the SLM but will be blocked by the slit mask. For $l = \pm 300$, only the section of the mode shown here was used in the measurements, because of the noise from diffraction at the SLM housing and distorted modulation due to the limitations of the finite resolution.

and the coincidence of two transmitted photons for different combinations of γ is measured.

In our experiment, polarization-entangled photon pairs (uncorrected average visibility 97.99 ± 0.03%) at 810 nm were created using a type II nonlinear crystal in a Sagnac-type configuration (*26*, *27*). The SLM in the transfer setup is programmed such that the reflected photons acquire l multiples of 2π azimuthal phase (l quanta of OAM), which leads to complex patterns when OAM is large (Fig. 1, B to D). Therefore, we used a high-resolution SLM (1920 × 1080, full HD; Holoeye Photonics AG, Berlin) with small pixel size (8 μm). Nonetheless, for values of $l \geq 300$ we observed a clear reduction of mode transformation efficiency, which is the main limiting factor (*22*). This is only a technical limitation that can be overcome by higher-resolution SLMs or novel techniques for creating photons with higher l values (*28*). After the transfer setups, the modes are enlarged to fit the masks (laser-cut black cardboard) and transmitted photons are focused to bucket detectors.

As a demonstration of the flexibility of our setup, we created two-dimensional spatial mode entanglement with highly asymmetric OAM states, in which one photon is transferred to $l = \pm 10$ and the second photon to $l = \pm 100$ (Fig. 3A). Because of its intrinsic conservation of angular momentum, the SPDC process could not create this asymmetric state directly. We then transferred both photons to $l = \pm 100$, showing the ability to create OAM modes with very high difference in quantum number (Fig. 3B). The highest value of OAM per single photon where strong correlations were still measurable was $l = \pm 300$ for both photons (Fig. 3C). The decrease in mode transformation efficiency of the SLM, however, strongly affects the coincidence rate (about 1 coincidence count per minute in the maximum) and therefore the statistical significance of our results.

To demonstrate successful transfer, we constructed an entanglement witness [similar to (*29*)], which verifies entanglement if the sum of two visibilities in two mutually unbiased bases is above the classical bound of $(2^{1/2} + 1)/2 \approx 1.21$ (*22*, *29*). The data for the visibilities were taken in addition to the fringe measurements (apart from $l = \pm 300$) with longer integration. For the asymmetric OAM state $l = \pm 10/\pm 100$, we achieved a witness value of 1.48 ± 0.01. When both photons were transferred to $l = \pm 100$, the witness value was 1.55 ± 0.01. Both values were calculated without any correction of the data and violate the classical limit by ~30 standard deviations, demonstrating the successful entanglement transfer. Because of the significantly smaller creation and detection efficiencies (hence a lower pair detection rate) for $l = \pm 300$, we corrected for accidental coincidence counts (*22*), yielding a value of 1.6 ± 0.3 for our entanglement witness. With a statistical significance of more than 80%, we thus violate the bound for separable states with photons that each carry $l = \pm 300$ quanta of OAM.

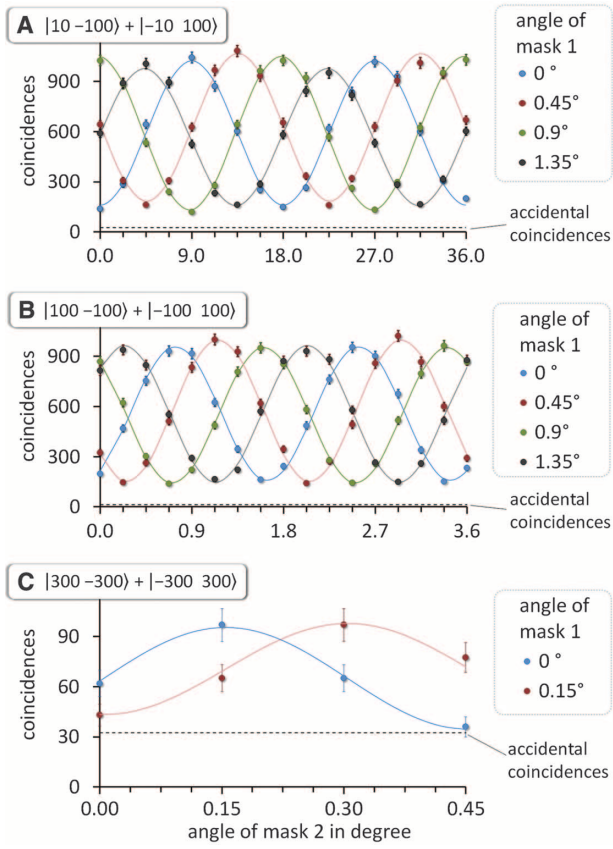

Fig. 3. Measured coincidence counts as a function of the angle of one mask and different angles of the other mask. The measured coincidence counts (points) show a sinusoidal dependence (fitted lines) and depend only on the difference between the angles of the masks, which is a clear signature of nonclassical correlations. (**A**) The first photon is transferred to $l = \pm 10\hbar$ and the second to $l = \pm 100\hbar$, showing the ability to create asymmetric OAM entangled states. (**B**) Both photons are transferred to $l = \pm 100\hbar$. (**C**) Both photons carry $l = \pm 300\hbar$ and nonclassical correlations can still be measured. Here, the count rate decreased significantly (about 1 coincidence count per minute) primarily because of limited conversion efficiency. The integration times in (A), (B), and (C) were 2 min, 9 min, and 64 min, respectively, for each data point. Error bars in all plots (if large enough to be seen) are estimated from Poissonian count statistics.

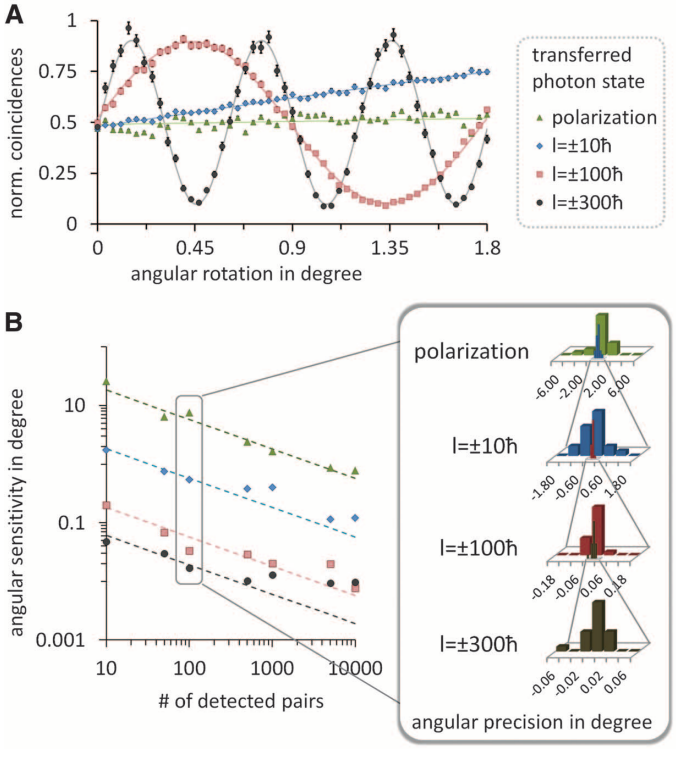

Fig. 4. Measurements of remote angular sensitivity enhancement. (**A**) Normalized coincidence count rates where one photon is projected on diagonal polarization, and the second photon is either kept polarization-encoded while the polarizer is rotated (green triangles) or transferred to $l = \pm 10\hbar$ (blue diamonds), to $l = \pm 100\hbar$ (red squares), or to $l = \pm 300\hbar$ (black circles) while the appropriate mask is rotated. The errors are estimated assuming Poissonian count statistics. (**B**) From the steepest part of the fringes (0°), it is possible to calculate the corresponding angular sensitivity limited by statistical fluctuations for different numbers of detected pairs. The dashed lines are the theoretically expected sensitivities (assuming 100% visibility and Poissonian fluctuation) and the points are the measured values. To illustrate the enhancement for 100 detected pairs, we measured the angular position of the randomly rotated mask by correcting the change in the coincidence counts with a rotation of the remote polarizer. The right panel shows histograms of 20 different random angles that were measured for each arrangement. For $l = \pm 300\hbar$, the limit of our high-precision rotation stage (±0.016°) was determined with the polarizer in a low-precision mount (±1°). To reach the same precision without OAM-induced angular resolution enhancement, about 3.3 million detected pairs would have been necessary.

To further corroborate this successful entanglement creation, we transferred only one photon to $l = \pm 300$ and measured the other photon in the polarization bases. The measured witness value was 1.628 ± 0.004. Therefore, our results demonstrate that single photons can carry $300\hbar$ of OAM (where $\hbar$ is Planck's constant divided by 2π) and that entanglement between two photons differing by 600 in quantum number can be achieved. Even in classical optics, the highest value of OAM that had been created with an SLM was $l = 200$ (*30*).

Apart from the fundamental interest of entangling high quantum numbers, we also demonstrate the use of high-OAM entanglement for remote sensing. For this we use the same method as before for creating high-OAM entangled states (folded interferometric scheme including SLM) and analyzing them (slit wheel method). When we transfer one photon to high OAM values and keep the other in its polarization state, the pair can be used to remotely measure an angular rotation with a precision that is increased by a factor l relative to the situation when only polarization-entangled photon pairs are used (Fig. 4) (*22*). This can lead to notable improvements for applications in the field of remote sensing, especially where low light intensities are required, such as in biological imaging experiments with light-sensitive material. An analogous improvement can be achieved classically if diagonally or circularly polarized light enters our transfer setup. However, the important difference is that entanglement enables the measurements to be done remotely, with the photons being spatially separated or even in unknown locations at some later time.

Our approach could be generalized to higher-dimensional entanglement for spatial modes—for example, by starting with higher-dimensional (hybrid) entanglement and a more complex interferometric scheme. Such a development would have potential benefits in applications such as quantum cryptography, quantum computation, and quantum metrology.

References and Notes

1. A. Einstein, B. Podolsky, N. Rosen, *Phys. Rev.* **47**, 777 (1935).
2. J. S. Bell, *Physics* **1**, 195 (1965).
3. S. J. Freedman, J. F. Clauser, *Phys. Rev. Lett.* **28**, 938 (1972).
4. P. G. Kwiat, A. M. Steinberg, R. Y. Chiao, *Phys. Rev. A* **47**, R2472 (1993).
5. A. Mair, A. Vaziri, G. Weihs, A. Zeilinger, *Nature* **412**, 313 (2001).
6. J. C. Howell, R. S. Bennink, S. J. Bentley, R. W. Boyd, *Phys. Rev. Lett.* **92**, 210403 (2004).
7. S. Ramelow, L. Ratschbacher, A. Fedrizzi, N. K. Langford, A. Zeilinger, *Phys. Rev. Lett.* **103**, 253601 (2009).
8. L. Allen, M. W. Beijersbergen, R. J. C. Spreeuw, J. P. Woerdman, *Phys. Rev. A* **45**, 8185 (1992).
9. N. K. Langford *et al.*, *Phys. Rev. Lett.* **93**, 053601 (2004).
10. J. Leach *et al.*, *Science* **329**, 662 (2010).
11. A. Vaziri, G. Weihs, A. Zeilinger, *Phys. Rev. Lett.* **89**, 240401 (2002).
12. A. C. Dada, L. Leach, G. S. Buller, M. J. Padgett, E. Andersson, *Nat. Phys.* **7**, 677 (2011).
13. B.-J. Pors, F. Miatto, G. W. 't Hooft, E. R. Eliel, J. P. Woerdman, *J. Opt.* **13**, 064008 (2011).
14. A. J. Leggett, *J. Phys. Condens. Matter* **14**, R415 (2002).
15. M. Aspelmeyer, P. Meystre, K. Schwab, *Phys. Today* **65**, 29 (2012).
16. A. K. Jha, G. S. Agarwal, R. W. Boyd, *Phys. Rev. A* **83**, 053829 (2011).
17. J. Romero, D. Giovannini, S. Franke-Arnold, S. M. Barnett, M. J. Padgett, http://arxiv.org/abs/1205.1968 (2012).
18. H. Di Lorenzo Pires, H. C. B. Florijn, M. P. van Exter, *Phys. Rev. Lett.* **104**, 020505 (2010).
19. M. Żukowski, J. Pykacz, *Phys. Lett. A* **127**, 1 (1988).
20. E. Nagali *et al.*, *Phys. Rev. Lett.* **103**, 013601 (2009).
21. E. J. Galvez, S. M. Nomoto, W. H. Schubert, M. D. Novenstern, paper presented at the International Conference on Quantum Information, Ottawa, 6 June 2011; www.opticsinfobase.org/abstract.cfm?URI=ICQI-2011-QMI18.
22. See supplementary materials on *Science* Online.
23. S. Chávez-Cerda *et al.*, *J. Opt. B* **4**, S52 (2002).
24. J. B. Bentley, J. A. Davis, M. A. Bandres, J. C. Gutiérrez-Vega, *Opt. Lett.* **31**, 649 (2006).
25. G. A. Siviloglou, J. Broky, A. Dogariu, D. N. Christodoulides, *Phys. Rev. Lett.* **99**, 213901 (2007).
26. T. Kim, M. Fiorentino, F. N. C. Wong, *Phys. Rev. A* **73**, 012316 (2006).
27. A. Fedrizzi, T. Herbst, A. Poppe, T. Jennewein, A. Zeilinger, *Opt. Express* **15**, 15377 (2007).
28. G. Campbell, B. Hage, B. Buchler, P. K. Lam, *Appl. Opt.* **51**, 873 (2012).
29. O. Gühne, G. Tóth, *Phys. Rep.* **474**, 1 (2009).
30. A. Jesacher, S. Fürhapter, C. Maurer, S. Bernet, M. Ritsch-Marte, *Opt. Express* **14**, 6342 (2006).

Acknowledgments: Supported by the European Research Council (advanced grant QIT4QAD, 227844) and the Austrian Science Fund (FWF) within the Special Research Programs (SFB) F40 (Foundations and Applications of Quantum Science; FoQuS) and W1210-2 (Vienna Doctoral Program on Complex Quantum Systems; CoQuS). R.F. participated in the design and building of the experimental apparatus, collected and analyzed the data, and wrote the manuscript. R.L., C.S., and S.R. participated in the design and building of the experiment and assisted on the experimental side. W.N.P., S.R., and M.K. assisted on the theoretical side. A.Z. initiated the work and supervised the experiment. All authors contributed to conceiving the experiment, discussing the results, and contributing to the final text of the manuscript.

Supplementary Materials

www.sciencemag.org/cgi/content/full/338/6107/640/DC1
Materials and Methods
Supplementary Text
Table S1
Fig. S1

9 July 2012; accepted 20 September 2012
10.1126/science.1227193

Efficient Hybrid Solar Cells Based on Meso-Superstructured Organometal Halide Perovskites

Michael M. Lee,[1] Joël Teuscher,[1] Tsutomu Miyasaka,[2] Takurou N. Murakami,[2,3] Henry J. Snaith[1]*

The energy costs associated with separating tightly bound excitons (photoinduced electron-hole pairs) and extracting free charges from highly disordered low-mobility networks represent fundamental losses for many low-cost photovoltaic technologies. We report a low-cost, solution-processable solar cell, based on a highly crystalline perovskite absorber with intense visible to near-infrared absorptivity, that has a power conversion efficiency of 10.9% in a single-junction device under simulated full sunlight. This "meso-superstructured solar cell" exhibits exceptionally few fundamental energy losses; it can generate open-circuit photovoltages of more than 1.1 volts, despite the relatively narrow absorber band gap of 1.55 electron volts. The functionality arises from the use of mesoporous alumina as an inert scaffold that structures the absorber and forces electrons to reside in and be transported through the perovskite.

An efficient solar cell must absorb over a broad spectral range, from visible to near-infrared (near-IR) wavelengths (350 to ~950 nm), and convert the incident light effectively into charges. The charges must be collected at a high voltage with suitable current in order to do useful work (*1*–*8*). A simple measure of solar cell effectiveness at generating voltage is the difference in energy between the optical band gap of the absorber and the open-circuit voltage (V_{oc}) generated by the solar cell under simulated air mass (AM) 1.5 solar illumination of 100 mW cm^{-2} (*9*). For instance, gallium arsenide (GaAs) solar cells exhibit V_{oc} of 1.11 V and an optical band gap of 1.4 eV, giving a difference of ~0.29 eV (*2*). For dye-sensitized and organic solar cells, this difference is usually on the order of 0.7 to 0.8 eV (*2*, *9*). For organic solar cells, such losses are predominantly caused by their low dielectric constants. Tightly bound excitons form, which require a heterojunction with an electron acceptor with a large energy offset to enable ionization and charge separation (*10*, *11*). Likewise, dye-sensitized solar cells (DSSCs) have losses, both from electron transfer from the dye (or absorber) into the TiO_2, which requires a certain "driving force," and from dye regeneration from

[1]Clarendon Laboratory, Department of Physics, University of Oxford, Oxford OX1 3PU, UK. [2]Graduate School of Engineering, Toin University of Yokohama, 1614 Kurogane, Aoba, Yokohama 225-8503, Japan. [3]Research Center for Photovoltaic Technologies, National Institute of Advanced Industrial Science and Technology, Central 5, 1-1-1 Higashi, Tsukuba, Ibaraki 305-8565, Japan.

*To whom correspondence should be addressed. E-mail: h.snaith1@physics.ox.ac.uk